Simulating Extensive Air Showers: Investigating the LDF for Electrons and Muons Using the AIRES System

Rawaa Y. Taha[*], Ahmed A. Al-Rubaiee, Itab F. Hussein

Department of Physics, College of Science, Mustansiriyah University, Baghdad 10011, Iraq

Corresponding Author Email: rawaa_yaseen@uomustansiriyah.edu.iq

ABSTRACT

Extensive air showers (EAS), cascades of electromagnetic radiation and ionized particles produced when primary cosmic rays (CRs) interact with atmospheric nuclei, generate a plethora of secondary particles, including electrons, muons, alpha particles, X-rays, and neutrons. These phenomena, pivotal in the exploration of high-energy CR interactions, have prompted advancements in simulating the lateral distribution function (LDF) of secondary particles. Utilizing AIR-shower extended simulations (AIRES) software (version 19.04.10), this study presents simulations of EAS to elucidate the impact on the LDF at the high energy thresholds of 1016, 1018 and 1019 eV. The focus is on secondary muons and electrons, considering the influence of primary protons and iron nuclei across zenith angles of 0°, 20°, and 40°. Through the application of an exponential function model, novel coefficients were derived, reflecting the variation of the LDF relative to the distance from the shower core. These coefficients are instrumental in astrophysics and particle physics, offering a nuanced understanding of CR interactions with earth's atmosphere. By delineating the spatial particle distribution during interactions, insights into the shower's lateral extent and configuration are gleaned, facilitating the deduction of the initiating CR's energy. Such knowledge is crucial for CR spectrum analysis. The investigation of electron and muon LDFs not only advances fundamental particle physics but also holds implications for space exploration, radiation protection, and other domains.

1. INTRODUCTION

EAS can be defined as a phenomenon resulting from the interaction of high-energy CRs with the earth's atmosphere. When high-energy CRs collide with an atom in the atmosphere's circumference, a set of secondary particles are produced through successive interactions, and these interactions continue and create more secondary particles before they reach the surface of the earth [1]. It has been observed that the series reaction of EAS reveals high-energy CRs produced in the atmosphere because some elementary particles cannot be detected directly but must be examined indirectly by consulting with the use of different measurement methods [2]. Pierre-Victor Auger [3], a French physicist, was the one who discovered this fact. The energy of the primary CRs is distributed among these secondary elements, resulting in the creation of an enormous cascade of particles until the energy of the EAS becomes insufficient to produce more particles in sequential collisions. This stage of the development of the shower is called the maximum shower [3, 4]. These secondary particles include electrons, positrons, muons, and photons. Each of them behaves differently and affects the development of showers through many factors, including the energy and composition of the primary CRs, the density of the atmosphere, and the evolution of the particle

numbers in the cascade. Therefore, LDF is formed as a function of atmospheric depth in a smooth curve at the maximum [5, 6]. Checking the EAS properties made by high-energy CRs is important for many reasons, but the main one is that understanding the nature of CRs is needed to explain high-energy astrophysical processes, and the EAS study helps researchers learn about the properties of CRs and the faraway astrophysical sources they create [7].

It is difficult to understand EAS due to complex interactions of particles within the atmosphere. Therefore, it requires knowledge of the shower evolution and the interaction mechanism of particles with air particles [8]. The interaction constantly decreases the level of energy possessed by the particles below their critical energy [9]. This energy represents the minimum energy needed by particles for their interaction with the atmosphere. In addition, it affects the ability of particles to interact effectively with air particles [10], and to detect these complexities and validate theoretical predictions. Therefore, extensive simulations are used. Monte Carlo simulation is defined as a computational technique, which uses different samples to calculate mathematical results and analyse systems. It involves creating inputs for a specific set of variables, applying them to a mathematical model or simulation, and then analysing the results. This simulation is widely used in many fields, including physics, engineering,

and other sciences [11].

Monte Carlo simulation is used to calculate LDF of high-energy particles because of the complexity of the air shower. The air shower contains a large number of secondary particles, and their interactions are affected by many factors, such as energy, the type of the main cosmic particle and the conditions of the atmosphere. Therefore, this simulation can be used to model these interactions in a random way. Along with the occurrence of the air shower in different atmospheric conditions, the LDF changes accordingly. The Monte Carlo simulation allows for the incorporation of variable parameters, such as altitude and density of the atmosphere and other factors. Thus, the simulations help to understand the development of the shower and identify the characteristics that can be observed at ground level and compare the results with experimental data. The LDF of the charged particle in the EAS is the quantity required to observe the cosmic radiation of the earth, which is mostly derived from EAS observations [12]. The EAS system evolves in a complex way from the combination of electromagnetic and hadronic showers. Therefore, it is important to make numerical data simulations to infer the properties of the primary CRs created. The number of high-energy particles in EAS can be tremendous and may exceed 10^{10}, which enables the simulation process to be the primary way to obtain the required information [13].

In this study, the density of charged particles LDF reaching the surface of the earth (electron and muon) was calculated as a function of the distance from the core of the shower using the AIRES system, where three high energies (10^{16}, 10^{18} and 10^{19}) eV were used for three zenith angles (0°, 20° and 40°). The angle was defined as the one between the path of the incident CR particle and the vertical axis extending directly upward from the observation point on earth's surface of the primary particles (proton, iron nuclei), where the effect of changing energy and angles on the density of secondary particles was discussed. Then the LDF equation was fitted and new coefficients were obtained for exponential function model. As a result of fitting the LDF function to the available data, a mathematical exponential function is created. The coefficients of the mathematical function are changed to be more like the actual values seen in the data. This creates a mathematical model that can be used to understand how the data behaves in general.

2. LATERAL DISTRIBUTION FUNCTION

LDF describes the density variation in secondary particles as a function of the distance from the axis of the shower. It determines the spatial distribution of particles inside the shower when these particles interact with the atmosphere. LDF is considered a tool for data analysis in particle physics. The study of cosmic interactions affected by factors includes the energy of the particles, the angle of their incidence and the type of particles. It can be represented in the form of mathematical equations based on specific parameters, where the equations determine how the number of particles changes with the distance. Thus, this contributes to the understanding of interactions and propagation of the cosmic beam in the exosphere, thereby determining the energy of these particles and the proportions of their interactions in the air [14]. One of the important EAS fundamentals at different distances from the central location is the density of particles charged through ground shower arrays, which can be calculated with extreme precision. It is important to focus on the lateral or radioactive

distribution function ρ(r) of different types of particles created in EAS in theoretical and experimental research since the discovery of EAS [14, 15]. It is necessary to solve the problem of LDF calculations of empirical data for large distances from the axis of the shower (r ≥ 1 km), through which experimental data on the air shower can be analyzed and new experiments updated to achieve reliable results at such large distances [16].

Calculating the LDF of electrons and muons for a CR includes several methods, including analytical models, empirical fits, and simulations. Therefore, using high-power EAS simulations is one of the most common methods as it gives an experimental overview based on multiple modifications. Thus, it is necessary to reconstruct the shower core in addition to the shower path itself and to know the LDF as well as compare it with model calculations for the details of the initial mass, which results in obtaining useful information. The fundamental reason why the LDF of EAS is important for the air shower phenomenon is that the mass and energy of the elementary particle can be calculated, and the ground particle distribution can also be obtained to correlate the primary energy of the particle with the mass, where more accurate algorithms need a comprehensive simulation of the air shower [17, 18]. To calculate the LDF of an electron, the common term NKG is used to describe this formula, which is one of the methods of analytical models and is given by the following equation [19]:

$$\rho_e(R) = \frac{N_e C(s)}{2\pi R_M^2} \left(\frac{R}{R_M}\right)^{s-2} \left(\frac{R}{R_M} + 1\right)^{s-4.5} \quad (1)$$

where, $\rho_e(R)$ represents the density of particles (electron), R represents the distance from the center of the shower, N_e is the number of electrons, s is the coefficient of the shower's age, $C(S)$ is the normalization coefficient, and R_M represents the Molière radii, which is a constant property of the material and whose value relies on the length of radiation (X) and its atomic number (z). The approximate relationship is presented as follows:

$$R_M = 0.0265X \cdot (z + 1.2) \quad (2)$$

The parameter s represents the age of the shower. Thus, the NKG function is effective within the range $0.8 < s < 1.6$, and $C(s)$ represents the normalization factor and equals 0.366 $(2.07-s)^{1.25}s^2$ [20].

3. HADRONIC AND ELECTRONIC SHOWER

The EAS consists of different shower cascade this can be classified into three cascades the electromagnetic, hadronic, muonic cascade. In the electromagnetic cascade, a simple model of Heitler was used, which is defined as the plainest concept of electromagnetic cascade. Proposed by Heitler [8], this model is a theoretical framework in particle physics, which describes the electromagnetic cascade initiated by high-energy CRs interacting with the earth's atmosphere. The model provides insights into the development of EAS by considering the successive generation of secondary particles resulting from electromagnetic interactions in the atmosphere. In the Heitler model, the primary CR, typically a high-energy photons or particle undergoes interactions with atmospheric nuclei. This leads to the production of electron-positron pairs through pair production, and subsequent energy loss occurs as

these particles emit photons via bremsstrahlung radiation. The cascade continues as the newly generated photons can, in turn, produce more electron-positron pairs through pair production, creating a sequence of successive generations of particles. Thus, Heitler's model predicted the importance of EAS properties. Figure 1(a) shows a single photon radiating using an electron after sending d the length of the split [13, 21]:

$$d = \lambda_r \ln 2 \qquad (3)$$

where, d represents the distance, where the electron misses out half of its energy in radiation, and λ_r represents the length of radiation in matter. After moving away for the same distance, it can be seen in both cases that the photon splits into a pair $e^{\pm}$. Assuming that the energy of the particle (photon or electron) is split between the two particles after n of the divisional lengths, the distance x is presented by the following equation:

$$x = n\lambda_r \ln 2 \qquad (4)$$

The overall volume of the electron and photon showers is as follows:

$$N = 2^n = e^{x/\lambda_r} \qquad (5)$$

The cessation of particle generation in EAS occurs when the energy of the particles becomes too low to produce the pair. Using Heitler's model, the electron energy is taken as critical energy and given by ξ_c^e. The rate of energy lost is greater than the radiation energy lost by collision.

If the shower begins with a single primary photon with the primary energy E_0, the cascade in the shower reaches its highest size ($N = N_{max}$) when the energy of the particles produced is equal to the critical energy (ξ_c^e), leading to the following equation:
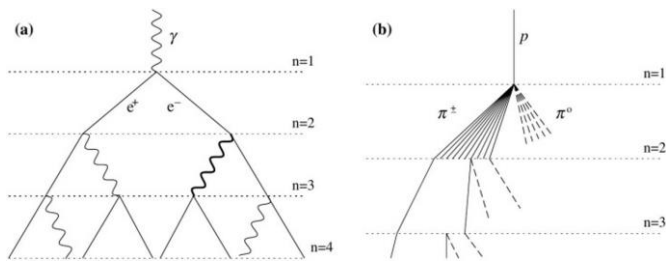
$$E_0 = \xi_c^e N_{max} \qquad (6)$$

Figure 1. Cascade caused by the Heitler model for (a) an electromagnetic shower and (b) a hadronic shower

It can be seen from Figure 1(a) that the air showers initiated by the hadrons were designed using a method similar to the Heitler model. Charged ($\pi^{\pm}$) and neutral (π^0) pions, which are defined as subatomic particles belonging to the family of muons, are the lightest mesons and, in general, the lightest hadrons, with a mass larger than that of an electron and smaller than that of a neutron. They are generated when protons interact with high-energy CRs in the earth's atmosphere. Hadron particles traverse one layer of the atmosphere, and the electromagnetic cascade begins after the neutral pions decay during this process into photon particles. Figure 1(b) shows that electromagnetic showers consist of the decomposition of neutral ions (dashed lines), whereas the charged pions ($\pi^{\pm}$) persist in reacting inside the shower until their energy is below

the critical energy of the pion (ξ_c^{π}). Therefore, the charged pions decompose into muons that reach the ground. The study of electromagnetic cascades is directly related to the LDF, as electromagnetic cascades are a series of interactions that occur when a high-energy charged particle collides with the earth's atmosphere. The LDF function describes how the energy of particles is distributed in an electromagnetic cascade, and can be used to determine the properties of cascades. The energy and type of CR particle are determined by measuring the characteristics of the electromagnetic cascade, such as its shape and size. LDF is used to determine the location of the initial reaction in the atmosphere by measuring the direction of the electromagnetic cascade [13].

4. AIRES SIMULATION

AIRES refers to a set of programs and subroutines that can be used to simulate and manipulate EAS particles generated by the interaction of high-energy native CRs with the environment [22]. AIRES simulates the full diffusion of space-time particles in a realistic environment, including the properties of the atmosphere and the earth's curvature and magnetic field. Statistical sample selection (thinning) is used when the number of particles in the showers is very high. The thinning algorithms of AIRES are equal, meaning that statistical sampling never changes the mean values of the observable outputs. A variety of particles are considered in AIRES simulations, including gamma, electrons, positrons, muons, mesons, pions, nucleons, antinucleons, lambda baryons, and nuclei up to Z=36. The elementary particle in EAS can be an elementary proton, an iron nucleus, or any of the previously mentioned particles (e-, e+, μ-, μ+, π-, π+), and its energy ranges from 10^9 eV to less than 10^{21} eV [23]. Thus, the AIRES simulation system involves fitting realistic simulations using existing computer technology. Total particles emitted by AIRES include the most commonly observed particles as well as a smaller number of species, which may indirectly have a minimal impact on the final observable shower. The AIRES simulation system consists of the following elements [22]:

♦ AiresSry: Summary software aims to process a subset of the data product through simulation, which allows the user to analyze the results after completion or even while working.

♦ Library Aries: Assists the user in processing compressed output data of files generated by the simulation software, writing external modules to handle custom primaries, etc. A group used to help. This library is implemented as an object library in UNIX environments.

♦ AIRES Operating System: A set of shell scripts that make working with AIRES in UNIX environments much easier. The standard structure of the main AIRES simulation program is shown schematically in Figure 2.

Therefore, it can be found that the details of the evolution of the shower are so complex that they can be fully determined through uncomplicated analytical modeling. In addition, the Monte Carlo simulation explained earlier is necessary for the interaction and transfer of each individual particle, thereby carrying out the evolution modeling of the shower used in the AIRES system.

The internal control procedures in the AIRES simulation engine examine particles, which touch the ground or move over the specified observation surfaces on the ground. The primary particle and its energy interacting with atmospheric atoms are determined after determining the number of showers.

Then the selection made is defined in addition to the kinetic energy of the electron and muon. Then the zenith angle and thinning energy are determined, and the observation planes are selected for the group that is used [24, 25].
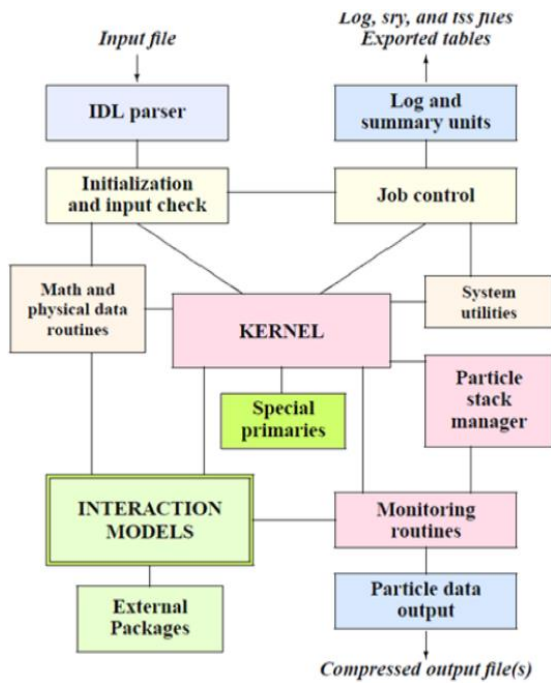

Figure 2. Structure of the AIRES simulation program

Many secondary particles are taken into account through simulation using the AIRES system, such as electrons, muons, gamma and positrons. The primary particle falling in the EAS may be a proton, iron nuclei, helium, or other elements fixed in the AIRES index with very high primary energies that may exceed 10^{21} eV [23]. Clearly, this fact was assured by the density graph of the air shower in relation to its core in the atmosphere with a certain energy value (10^{16}, 10^{18} and 10^{19}) eV. After conducting the simulation and obtaining the results, conclusions were drawn using the Originlab program. It was

noted from the drawings that there was a difference in the behavior of the LDF when changing the energy, angle, and type of elementary particles. Thus, the LDF was calculated as a function of the distance from the shower axis [9].

5. RESULTS AND DISCUSSIONS

Figures 3 and 4 show the density of three secondary particles (e, μ+, and μ-) as a distance function from the shower axis to the surface of the earth. The impact of primary particles (p, Fe) and energies (10^{16}, 10^{18}, and 10^{19}) eV on LDF is evident for different zenith angles. It can be seen from the figure that the LDF of the secondary particles decreases with increasing distance from the shower axis because particles constantly interact with atmospheric particles, leading to energy loss and direction change. The particles become more diffuse as they travel through the atmosphere. It can be noted that the density is higher at the shower axis and decreases continuously with the spread of particles. It turns out that LDF for electrons is higher than that for muons and anti-muons at all distances from the shower axis because electrons are lighter than muons and anti-muons, leading to more interaction with the atmosphere. As a result, electrons lose energy more quickly and become more diffuse. Muons suffer from less dispersion than electrons and lose less energy to particles in the atmosphere because of their higher mass. In addition, they are less affected by the earth's magnetic field than electrons, and are more likely to reach the surface of the earth. As a result, LDF for muons is less than that for electrons. The figures also show the energy effect of the primary particle as the energy of the particles increases. The primary particles with higher energies produce more secondary particles as they interact with the atmosphere. As for the zenith angle effect, the particle density is higher for low zenith angles because low-angle particles have more time to interact with atmospheric particles and thus produce more secondary particles. Interpreting these results is important in understanding how CRs interact with the atmosphere and deducing the dependence of LDF on the energy, type of the elementary particle, and zenith angle.
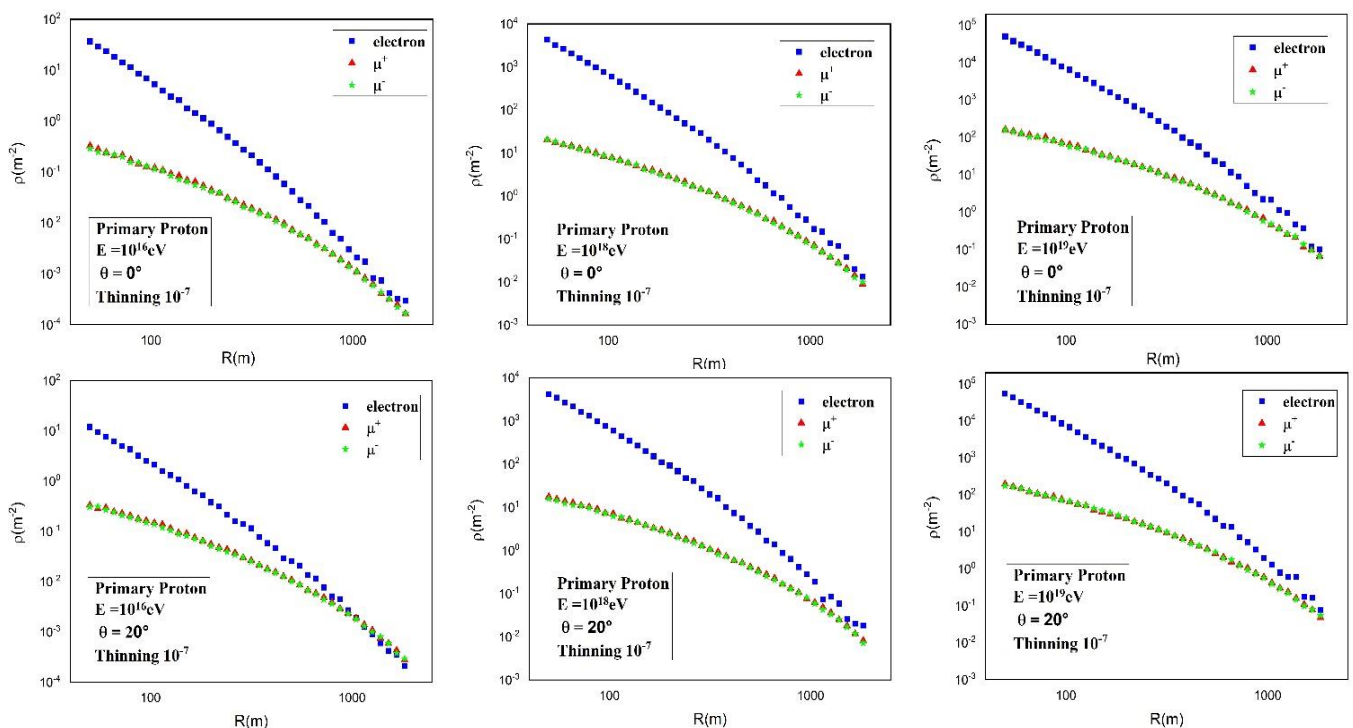
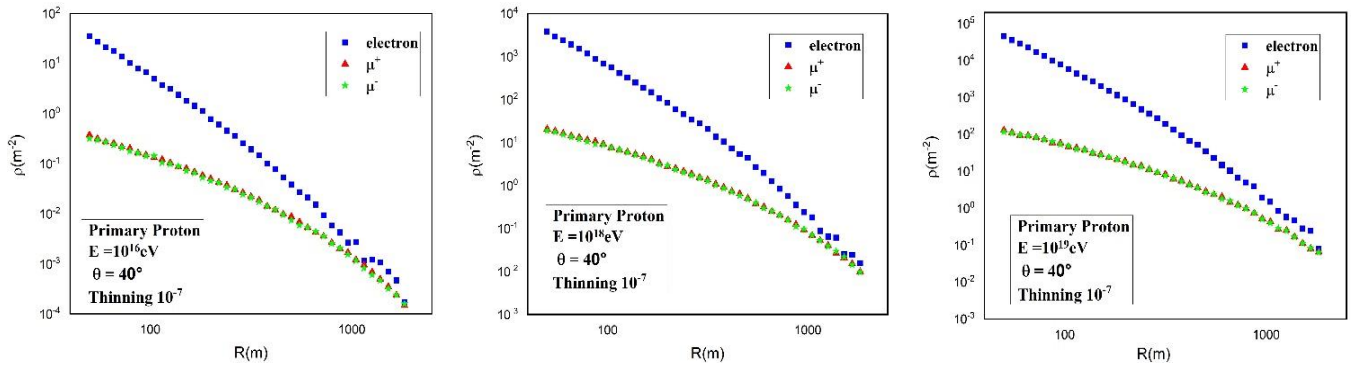**Figure 3.** LDF of secondary particles as a distance function from the shower axis of the primary particle (proton)
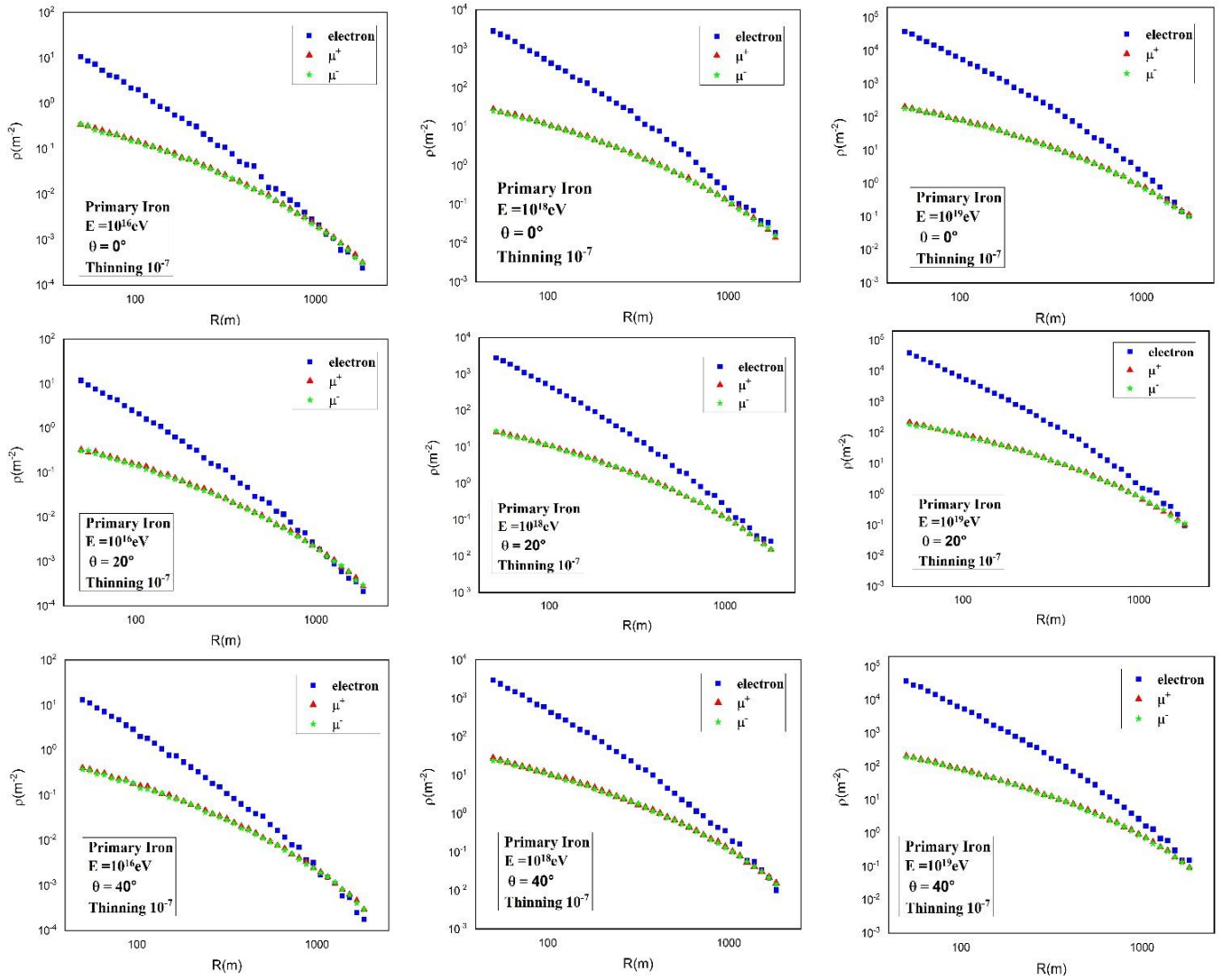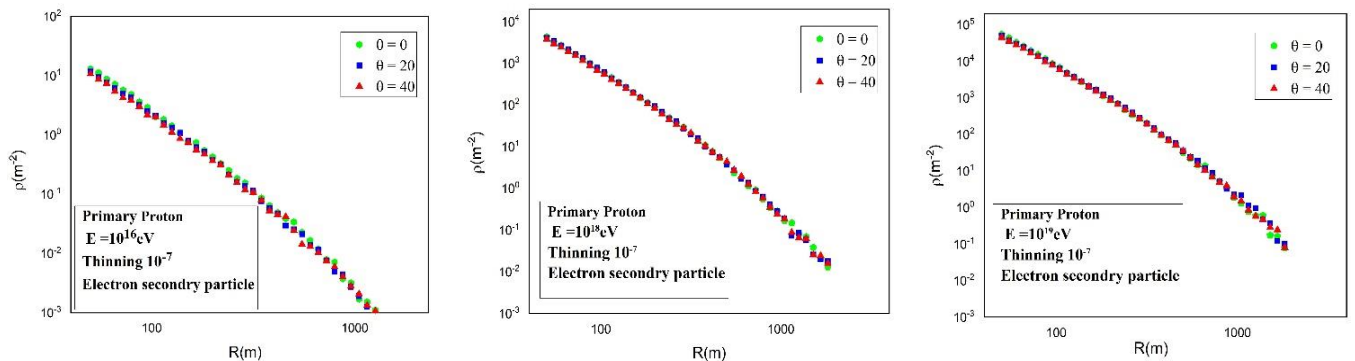

Figure 4. LDF of secondary particles as a distance function from the shower axis of the primary particle (iron nuclei)
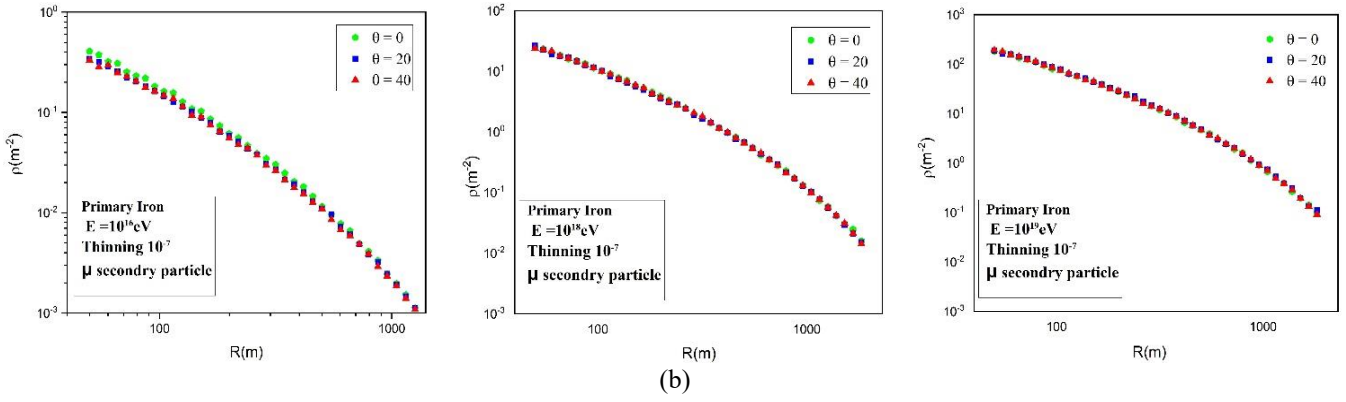

(a)

(b)

Figure 5. Effect of zenith angle on lateral density for primary particles (p, Fe)

Figure 5(a) and Figure 5(b) show the LDF of particles in EAS at different energy values and different zenith angles. LDF is higher at a close distance from the core of the shower. The top of the LDF becomes wider and farther as the energy of the primary particle increases, because high-energy particles produce more secondary particles as they interact with the atmosphere, and these particles are spread over a larger area. LDF is affected by the change in angle. It can be noticed that when the angle increases, the LDF decreases and its peak moves closer to the core of the shower due to the presence of fewer particles in the EAS, which have moved through a thicker layer in the atmosphere. As a result of air absorption, the number of particles in the shower reduces. It can be concluded that the effective length that represents the distance traveled by the shower through the atmosphere is longer for the oblique shower than that for the vertical shower. The oblique shower travels through a thicker layer in the atmosphere. Therefore, the longer effective length gives the shower enough time to develop, and the shower looks older when it hits the ground. The maximum development of EAS is the main point for the development of the shower. At this point, the number of particles in the shower is as large as possible. This point is reached at a certain distance from the core of the shower. Then it limits the number of particles in the shower, leading to their energy reduction and loss due to interaction with air molecules. It can be concluded from these results that it is important and necessary to understand the influencing factors, thereby analyzing and interpreting EAS data and providing information on the properties of the primary particles and the process of developing the shower.

6. LDF PARAMETERIZATION

An AIRES simulation was performed for the primary particles (p, Fe) with energies (10^{16}, 10^{18}, and 10^{19} eV) and an LDF calculation. The exponential function model was used to fit the LDF initiated in the EAS and obtain three new parameters of the primary particle that depend on the type and energy of the primary particles created in the EAS.

Table 1. Values of new coefficients for the primary proton

Primary Particles	$\theta°$	Energy	Secondary Particles	Values of Coefficients					R^2
				$\rho_\circ$	α_1	β_1	α_2	β_2	
		10^{16}	e	510.2	-25.48	57.32	-484.69	17.08	0.999
			μ^+	1.873	-1.607	21.05	-0.263	112.66	0.996
			μ^-	0.776	-0.667	41.51	-0.108	175.63	0.997
		10^{18}	e	1079.7	-102.08	13.33	-554.82	45.18	0.999
P	0°		μ^+	65.73	-54.31	32.63	-11.34	139.97	0.999
			μ^-	101.36	-84.88	23.11	-16.34	111.42	0.999
		10^{19}	e	1.343	-746.27	41.44	-1.268	13.09	0.999
			μ^+	453.03	-381.75	39.43	-70.81	155.97	0.998
			μ^-	574.45	-474.98	29.80	-98.75	129.47	0.998
		10^{16}	e	510.21	-25.48	57.32	-484.69	17.08	0.999
			μ^+	1.873	-1.607	21.05	-0.263	112.66	0.996
			μ^-	0.776	-0.667	41.51	-0.108	175.63	0.997
		10^{18}	e	4437.3	-190.47	64.70	-424.15	19.48	0.999
P	20°		μ^+	54.41	-45.51	34.92	-8.833	148.43	0.998
			μ^-	46.76	-10.19	133.61	-36.50	33.88	0.998
		10^{19}	e	1.008	-475.01	48.14	-960.98	15.43	0.999
			μ^+	1537.3	-136.12	18.54	-167.67	97.62	0.998
			μ^-	770.12	-650.61	26.67	-118.86	120.71	0.998
		10^{16}	e	878.95	-46.03	46.059	-832.85	13.29	0.999
			μ^+	1.958	-0.279	115.84	-1.676	22.47	0.998
			μ^-	0.989	-0.817	35.48	-0.170	146.74	0.998
		10^{18}	e	5209.1	-305.74	53.99	-490.78	16.94	0.999
P	40°		μ^+	71.08	-59.21	31.71	-11.70	139.79	0.999
			μ^-	75.04	-60.64	26.96	-14.246	122.23	0.999
		10^{19}	e	6019.5	-574.27	17.57	-271.68	57.13	0.999
			μ^+	464.55	-383.63	29.51	-80.32	130.96	0.997
			μ^-	312.05	-45.24	176.55	-266.5	42.80	0.999

Table 2. Values of new coefficients for the primary iron nuclei

| Primary Particles	$\theta°$	Energy	Secondary Particles	$\rho_{\circ}$	α_1	β_1	α_2	β_2	R^2
						Values of Coefficients			
		10^{16}	e	134.16	-7.952	62.94	-126.19	17.34	0.998
			μ^+	1.098	-0.882	32.63	-0.213	147.60	0.999
			μ^-	2.764	-0.312	114.19	-2.448	17.69	0.997
		10^{18}	e	2549.7	-786.46	83.07	-2471.0	21.65	0.999
Fe	0°		μ^+	91.24	-75.20	32.32	-15.91	139.43	0.997
			μ^-	83.70	-67.69	32.00	-15.87	137.03	0.999
		10^{19}	e	4796.4	-1872.8	64.80	-4609.6	18.17	0.999
			μ^+	928.57	-167.71	113.75	-759.45	23.92	0.998
			μ^-	551.33	-457.66	36.89	-93.04	153.97	0.998
		10^{16}	e	194.48	-181.15	15.04	-13.31	53.84	0.999
			μ^+	0.801	-0.150	174.55	-0.649	44.44	0.997
			μ^-	0.903	-0.749	38.48	-0.152	171.16	0.997
		10^{18}	e	3169.2	-1427.1	65.93	-3026.7	18.85	0.999
Fe	20°		μ^+	79.07	-65.76	35.72	-13.21	152.62	0.999
			μ^-	119.29	-99.32	24.43	-19.78	117.23	0.997
		10^{19}	e	6769.4	-649.99	15.83	-2751.9	56.50	0.999
			μ^+	1404.2	-193.27	105.74	-120.37	19.52	0.998
			μ^-	486.42	-414.99	43.14	-71.06	180.79	0.998
		10^{16}	e	110.08	-5.261	77.99	-104.73	21.58	0.999
			μ^+	1.380	-0.262	137.61	-1.115	30.90	0.998
			μ^-	1.311	-0.256	136.02	-1.052	29.77	0.997
		10^{18}	e	5860.7	-552.5	14.46	-339.76	49.03	0.999
Fe	40°		μ^+	143.91	-122.19	22.68	-21.54	117.57	0.999
			μ^-	69.31	-58.41	39.45	-10.82	168.77	0.998
		10^{19}	e	4229.7	-621.62	18.48	-213.29	60.24	0.998
			μ^+	684.05	-577.84	33.80	-105.38	145.44	0.999
			μ^-	638.84	-539.23	33.88	-98.86	147.28	0.999

Several functions have been applied and found to be suitable for electrons and muons at the same time, and this function is given in the following form:

$$\rho_{\circ}=\rho_{\circ}+\alpha_1\left(1-\exp\left(\frac{-R}{\beta_1}\right)\right)+\alpha_2\left(\frac{-R}{\beta_2}\right) \qquad (7)$$

where, ρ represents the shower density in EAS; α, β and $\rho_{\circ}$ represent the LDF coefficients as shown in Tables 1 and 2. These coefficients are obtained by fitting the results of the simulation using the AIRES system.

Figures 6 and 7 show the parameterization of the simulated LDF for (e, $\mu+$, $\mu-$) in EAS using the AIRES system. The results are presented for the primary particle (p, Fe) at energies (10^{16}, 10^{18}, and 10^{19} eV) with three zenith angles ($\theta = 0°$, $20°$ and $40°$) (symbol) and the results obtained using Eq. (7) (solid line) for the energy thinning 10^{-7} Re. LDF, which describes the density of secondary particles as a function of the distance from the shower axis, was calculated using the exponential function model that effectively described LDF in EAS.
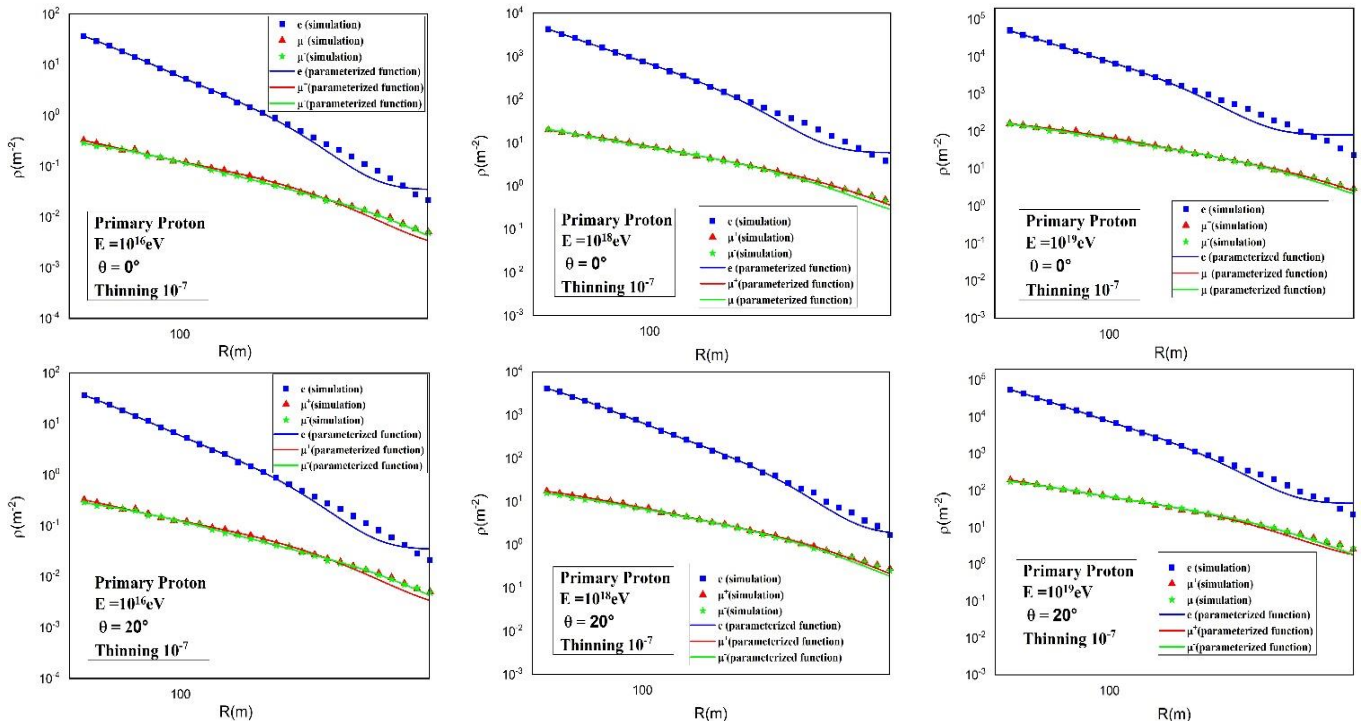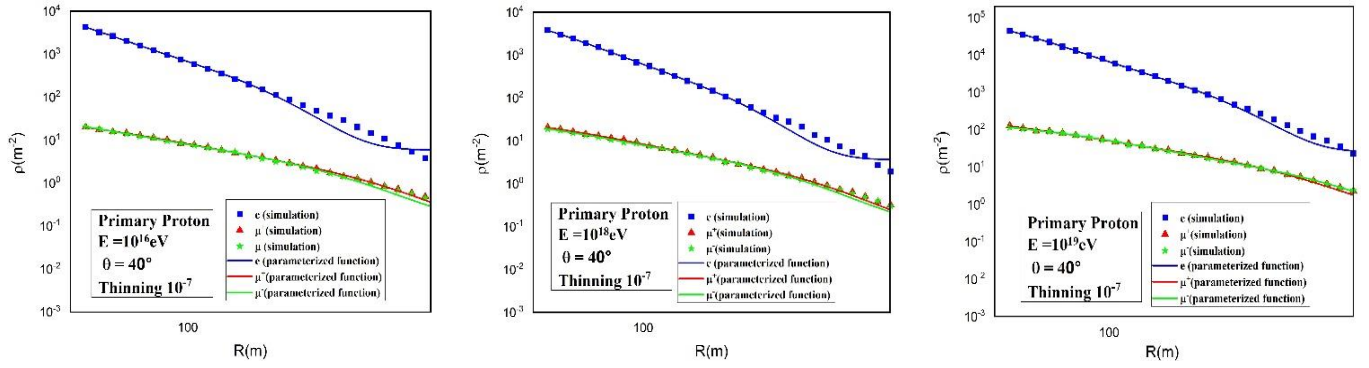
Figure 6. LDF simulated using the AIRES system (symbol) with the results obtained using Eq. (7) (solid line) for the primary proton particle
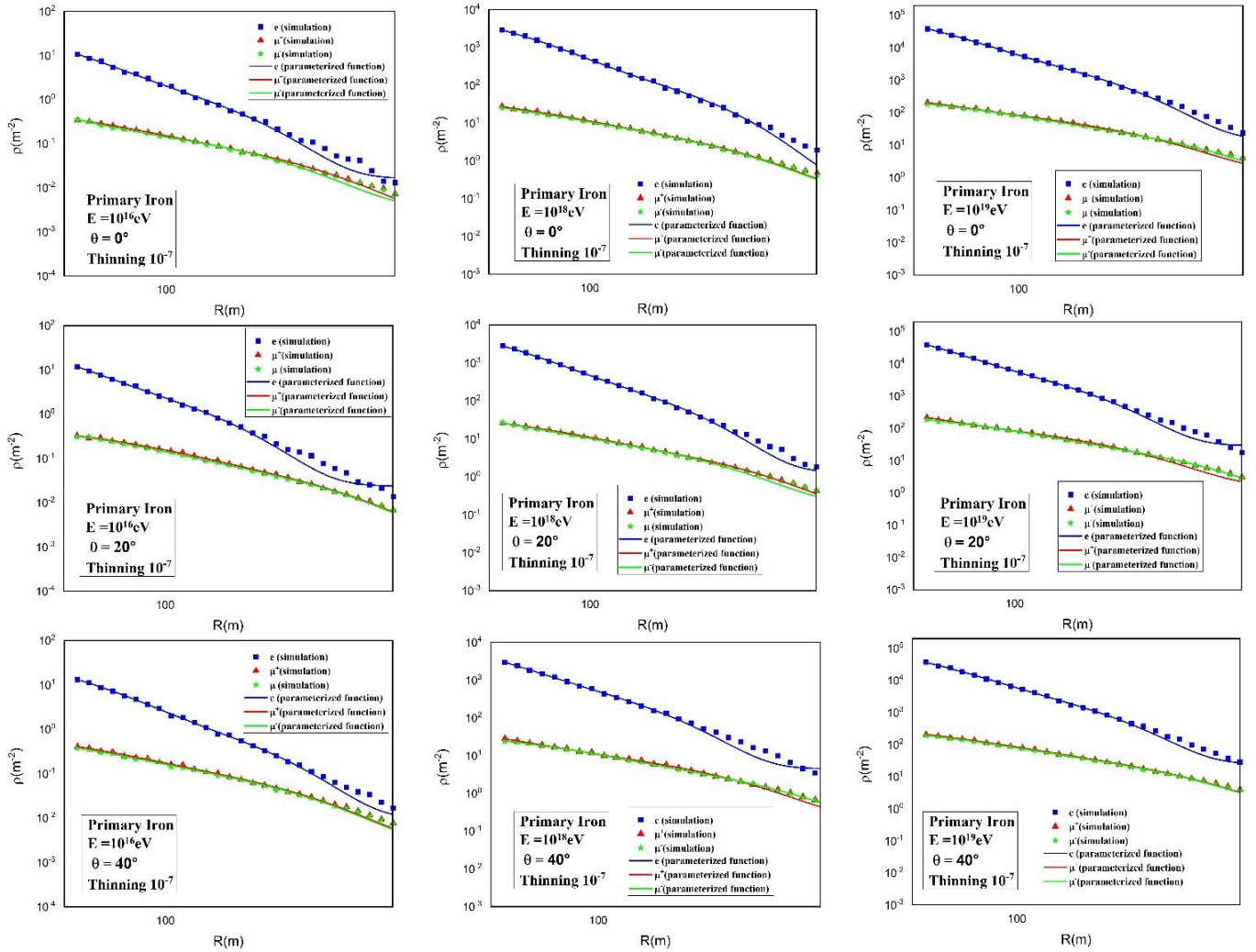

Figure 7. LDF simulated using the AIRES system (symbol) with the results obtained using equation 7 (solid line) for the primary particle iron nuclei

A good agreement between the simulation curves and the fitting curves of the LDF can be observed, which confirms the effectiveness of the exponential function model. It can be noted that the function model is more accurate for muons compared to electrons due to the depth of their penetration into the atmosphere. The most pronounced fluctuations that affect LDF and their behavior are similar for all particles. The peak density is close to the shower core, followed by a gradual decrease when the distance from the shower core increases. This function resulted in three new parameters, from which the properties of the elementary particle, such as its type and energy, can be deduced. The properties are important in the study of cosmic radiation formation, particle transport processes, and interaction in EAS.

7. COMPARISON OF THE SIMULATED LDF WITH THE SCIUTTO DATA

Figure 8 shows the compared results between the simulated LDF obtained using AIRES (square blue symbols) and the calculated results by Sciutto (square red symbols) [23]. This

comparison shows similarity in behavior for the secondary particles of electrons and muons produced by the primary proton at a fixed primary energy of 10^{19} eV. The results obtained using the AIRES program showed good compatibility with the results of Sciutto for proton particles with a thinning of 10^{-7} for vertical EAS showers.
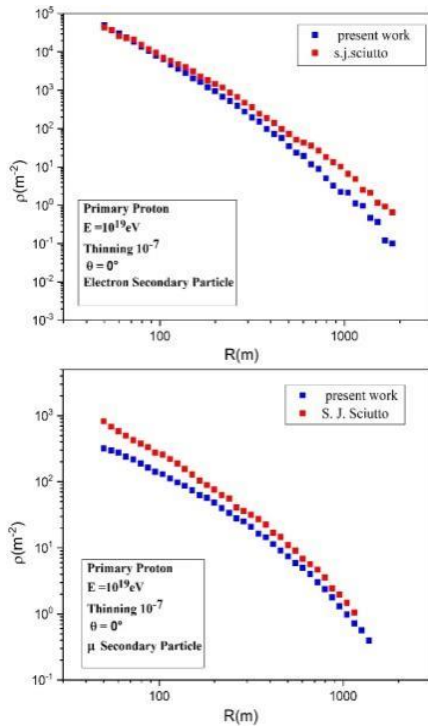

Figure 8. Comparison of the simulated results of LDF with the results for primary proton estimated by Sciutto

The study of LDF simulation of electrons and muons in EAS has several plans for future studies:

1. LDF simulations can be performed using different secondary particles, such as ions, photons, and kaons.
2. Study the effect of various factors on the LDF, such as temperature and pressure.
3. Investigation of the reasons that lead to the density reduction of secondary particles at a greater distance from the shower axis.
4. More sophisticated simulation programs can be created for EAS, which incorporate the latest physical models and experimental data.
5. The results of the LDF using AIRES simulation can be compared with those of LDF simulation using another program, such as CORSEKA.
6. Calculation of LDF using different elementary particles, such as carbon and helium, for different angles and energies above 10^{20} eV.

8. CONCLUSIONS

The simulation of the LDF of charged particles in the EAS was performed using the AIRES system of the primary particles (proton, iron nuclei) for three different high energies (10^{16}, 10^{18}, and 10^{19}) eV and three different zenith angles ($\theta = 0°$, $20°$, and $40°$). The results of the study showed that using the LDF function, it is possible to understand the characteristics of the air shower and conclude that this function

is affected by various factors, including energy, particle type, and incidence angle. It is noted that the LDF decreases as the distance from the shower axis increases. In addition, the LDF is higher at the shower axis, and then gradually decreases due to the continuous interactions of particles with atmospheric molecules. As a result, these particles lose their energy. Therefore, the trends are changing and the spread is increasing. The LDF of electrons is higher than that of muons at all distances because electrons are lighter and easily deflected by the earth's magnetic field, interact more with the atmosphere, and lose energy very quickly. It can be concluded from this study that the density of secondary particles is directly proportional to the energy of the primary particle. The greater the energy of the particle, the greater the LDF, because high-energy particles produce more secondary particles through their interaction with the atmosphere. As for the effect of zenith angles, it can be noted that LDF is higher at low angles because the particles moving at low angles have more time to interact with particles in the atmosphere, and the production of secondary particles increases. New parameters were obtained for the fitting procedure of the LDF using the exponential function model, and these parameters helped to determine the properties of the shower and estimate the energy of the CR, in addition to their importance in the disciplines of astrophysics and particle physics. The comparison made in the study shows similarity in behavior for the secondary particles of electrons and muons produced by the primary proton at a fixed primary energy of 10^{19} eV. The results obtained using the AIRES program showed good compatibility with those of Sciutto for proton particles with a thinning of 10^{-7} for vertical EAS showers. It shows an opportunity for primary energy definition and identification of primary particles in the CR energy spectrum.

REFERENCES

[1] Aab, A., Abreu, P., Aglietta, M., et al. (2019). Measurement of the average shape of longitudinal profiles of cosmic-ray air showers at the Pierre Auger Observatory. Journal of Cosmology and Astroparticle Physics, 2019(3): 018. https://doi.org/10.1088/1475-7516/2019/03/018

[2] Holt, E.M., Pierre Auger Collaboration. (2016). The auger engineering radio array and multi-hybrid cosmic ray detection. Journal of Physics: Conference Series, 718(5): 052019. https://doi.org/10.1088/1742-6596/718/5/052019

[3] Bhatnagar, S. (2009). Extensive Air Shower High Energy Cosmic Rays (II). Physics Education, pp. 249-256.

[4] Longair, M.S. (2010). High Energy Astrophysics. Cambridge University Press.

[5] Swordy, S.P., Kieda, D.B. (2000). Elemental composition of cosmic rays near the knee by multiparameter measurements of air showers. Astroparticle Physics, 13(2-3): 137-150. https://doi.org/10.1016/S0927-6505(99)00117-6

[6] Fowler, J.W., Fortson, L.F., Jui, C.C.H., et al. (2001). A measurement of the cosmic ray spectrum and composition at the knee. Astroparticle Physics, 15(1): 49-64. https://doi.org/10.1016/S0927-6505(00)00139-0

[7] Cillis, A.N., Sciutto, S.J. (2001). Extended air showers and muon interactions. Physical Review D, 64(1): 013010. https://doi.org/10.1103/PhysRevD.64.013010

[8] Risse, M. (2004). Properties of extensive air showers.

arXiv preprint astro-ph/0402300. https://doi.org/10.48550/arXiv.astro-ph/0402300

[9] Fadhel, K.F., Al-Rubaiee, A.A., Jassim, H.A., Al-Alawy, I.T. (2021). Estimating the lateral distribution of high energy cosmic ray particles by depending on Nishimura-Kamata-Greisen function. Journal of Physics: Conference Series, 1879(3): 032089. https://doi.org/10.1088/1742-6596/1879/3/032089

[10] Knurenko, S.P., Ivanov, A.A., Pravdin, M.P., Sabourov, A.V., Sleptsov, I.Y. (2008). Recent results from the Yakutsk experiment: The development of EAS and the energy spectrum and primary particle mass composition in the energy region of 10 15 10 19 eV. Nuclear Physics B Proceedings Supplements, 175: 201-206. https://doi.org/10.1016/j.nuclphysbps.2007.10.035

[11] Roth, M. (2003). The lateral distribution function of shower signals in the surface detector of the Pierre auger observatory. arXiv preprint astro-ph/0308392. https://doi.org/10.48550/arXiv.astro-ph/0308392

[12] Haungs, A., Rebel, H., Roth, M. (2003). Energy spectrum and mass composition of high-energy cosmic rays. Reports on Progress in Physics, 66(7): 1145. https://doi.org/10.1088/0034-4885/66/7/202

[13] Matthews, J. (2005). A Heitler model of extensive air showers. Astroparticle Physics, 22(5-6): 387-397. https://doi.org/10.1016/j.astropartphys.2004.09.003

[14] Lagutin, A.A., Raikin, R.I., Inoue, N., Misaki, A. (2002). Electron lateral distribution in air showers: scaling formalism and its implications. Journal of Physics G: Nuclear and Particle Physics, 28(6): 1259. https://doi.org/10.1088/0954-3899/28/6/309

[15] Ivanov, A.A. (2017). Zenith angle distribution of cosmic ray showers measured with the Yakutsk array. In 35th International Cosmic Ray Conference, Bexco, Busan, Korea.

[16] Lagutin, A.A., Raikin, R.I. (2001). Lateral distribution of electrons in EAS at superhigh energies: Predictions and experimental data. Nuclear Physics B-Proceedings Supplements, 97(1-3): 274-277.

[17] Barnhill, D., Bauleo, P., Dova, M.T., et al. (2005). Measurement of the lateral distribution function of UHECR air showers with the Pierre Auger observatory. arXiv preprint astro-ph/0507590. https://doi.org/10.48550/arXiv.astro-ph/0507590

[18] Antoni, T., Apel, W.D., Badea, F., et al. (2001). Electron, muon, and hadron lateral distributions measured in air showers by the KASCADE experiment. Astroparticle Physics, 14(4): 245-260. https://doi.org/10.1016/S0927-6505(00)00125-0

[19] Bartoli, B., Bernardini, P., Bi, X.J., et al. (2016). Detection of thermal neutrons with the PRISMA-YBJ array in extensive air showers selected by the ARGO-YBJ experiment. Astroparticle Physics, 81: 49-60. https://doi.org/10.1016/j.astropartphys.2016.04.007

[20] Jassim, H.A., Al-Rubaiee, A.A., Al-Alawy, I.T. (2020). Theoretical study of extensive air shower effects in atmosphere by simulating the lateral structure of several cosmic radiations. arXiv preprint arXiv:2007.16004. https://doi.org/10.48550/arXiv.2007.16004

[21] Leroy, C., Rancoita, P.G. (2000). Physics of cascading shower generation and propagation in matter: Principles of high-energy, ultrahigh-energy and compensating calorimetry. Reports on Progress in Physics, 63(4): 505. https://doi.org/10.1088/0034-4885/63/4/202

[22] Sciutto, S.J. (1999). AIRES: A system for air shower simulations. arXiv preprint astro-ph/9911331. https://doi.org/10.48550/arXiv.astro-ph/9911331

[23] Sciutto, S. (2002). AIRES User's Manual and Reference Guide, version 2.6. http://www.fisica.unlp.edu.ar/auger/aires.

[24] Ostapchenko, S. (2011). Monte Carlo treatment of hadronic interactions in enhanced Pomeron scheme: QGSJET-II model. Physical Review D, 83(1): 014018.

[25] Pierog, T., Karpenko, I., Katzy, J.M., Yatsenko, E., Werner, K. (2015). EPOS LHC: Test of collective hadronization with data measured at the CERN Large Hadron Collider. Physical Review C, 92(3): 034906.

https://doi.org/10.1016/S0920-5632(01)01282-8